Chapter 4
Lattice Boltzmann Method for Acoustics Levitation

Xiao-Peng Chen

Abstract In this chapter, a novel computational method for flow, lattice Boltzmann method, is introduced. We first present the fundamentals and general implements of the method, followed by non-reflective boundary condition techniques, which is important for acoustic simulations. The von Neumann analysis shows lattice Boltzmann method is promising for acoustic simulations. In the latter part of this chapter, we present the applications of lattice Boltzmann method on sound phenomena, such as aeroacoustics, non-linear sound effect and acoustic levitation.

4.1 Introduction

Sound generation and propagation have inherent fundamentals of fluid dynamics, where the media carrying sound waves is considered as a compressible fluid. It is shown that the simplest wave equation can be derived from the governing equations of fluid dynamics (Navier–Stokes/N–S equations) with the assumption of extremely small density and velocity fluctuation [1]:

$$\frac{\partial^2 \phi}{\partial t^2} - c^2 \nabla \phi = 0. \tag{4.1}$$

In the equation, ϕ denotes velocity potential: $\boldsymbol{u'} = -\nabla\phi$, and $c = \sqrt{(\partial p/\partial \rho)_s}$ is speed of sound. The disturbed pressure is $p' = -\rho_0 \partial\phi/\partial t$. It is also revealed that acoustic energy is propagated with sound wave: $E = \frac{1}{2}\rho_0 u'^2 + \frac{1}{2}\frac{c^2\rho'^2}{\rho_0}$. In this chapter, we denote the deviations of the respective quantities from their equilibrium values, which are denote with the subscript "0", by using primed letters. Non-linear effects can be further explored by taking account of the second-order terms ($O\left(M^2\right)$, $M = \left|\boldsymbol{u}'\right|/c$) in the N–S equations [2]. Burger's equation is applicable (in one-dimensional space):

X.-P. Chen (✉)
School of Marine Science and Technology, Northwestern Polytechnical University, 710072 Xi'an, Shaanxi, China
e-mail: xchen76@nwpu.edu.cn

D. Zang (ed.), *Acoustic Levitation*,
https://doi.org/10.1007/978-981-32-9065-5_4

$$\frac{\partial u'}{\partial t} + u' \frac{\partial u'}{\partial x} = \nu \frac{\partial^2 u'}{\partial x^2}, \tag{4.2a}$$

which successfully predicts the occurrence of shockwave from a sinusoidal wave, and ν is viscosity. The last term on the right-hand side represents a dissipation effect. Combined with mass conservation equation, it can be recast as

$$\frac{\partial^2 u'}{\partial t^2} - \left(c^2 + \nu \frac{\partial}{\partial t} \right) \frac{\partial^2 u'}{\partial x^2} = 0. \tag{4.2b}$$

Although the linear sound theory achieves great successes in sound prediction, the mechanical fundamentals of sound are still worthy of studying in many complicated situations. One of the notable subjects is aeroacoustics, which normally refers to the study on noise generation via either turbulent flow or aerodynamic forces interacting with surfaces. The topics include the aeolian tones produced by wind blowing over fixed objects. Starting from N–S equations, the celebrated Lighthill equation of aeroacoustics is derived without any additional assumptions:

$$\frac{\partial^2 \rho}{\partial t^2} - c_0^2 \nabla^2 \rho = \nabla \nabla : \boldsymbol{T}, \tag{4.3}$$

where $\boldsymbol{T}$ is the Lighthill stress tensor (second-order tensor). The last term in the equation is the source term, which can also include monopole, dipole and quadrupole motions of the fluid depending on flow conditions [3–5]. On the other hand, almost all the studies on non-linearity of sound phenomena root in N–S equations, while different mathematical approaches are applied [6, 7].

Therefore, well-developed numerical methods on fluid dynamics, known as Computational Fluid Mechanics (CFD), are supposed to be valuable in acoustic studies. In this chapter, lattice Boltzmann method, a promising numerical method, is to be introduced, and its applications on acoustics and acoustic levitations will be included as well.

4.2 Fundamentals on Lattice Boltzmann Method (LBM)

4.2.1 Governing Equations and Mathematics

It has been realized that the particle dynamics in a massive system can be applied to recover fluid flow. For these particle systems, various numerical approaches are developed, such as smooth particle hydrodynamics (SPH), molecular dynamics (MD) and moving particle semi-implicit method (MPS). A slightly different method is lattice Boltzmann method (LBM), which could be obtained from the classical Boltzmann equation (Fig. 4.1):

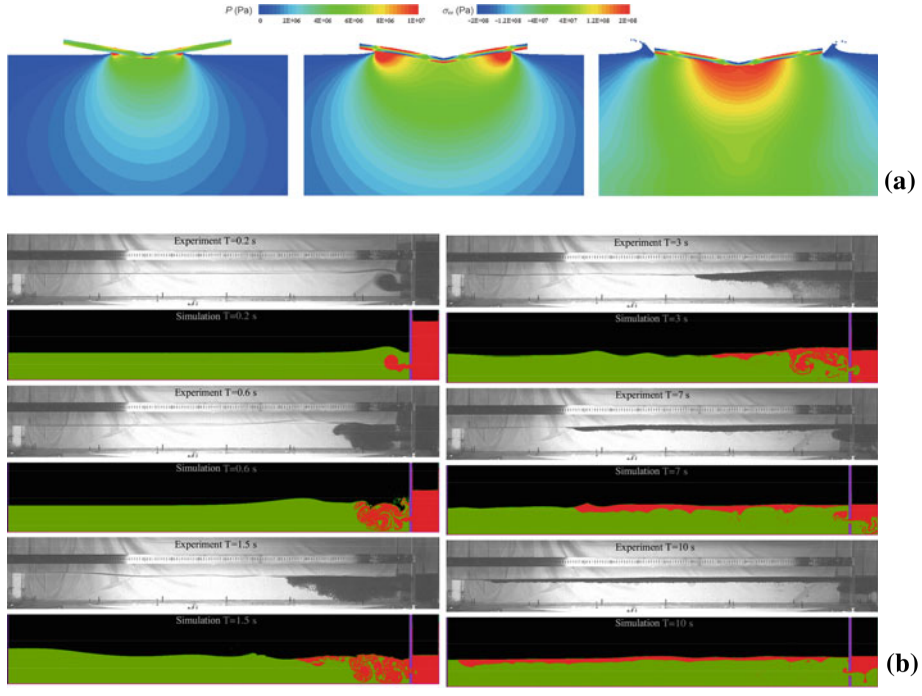

Fig. 4.1 Computational results from particle-based methods. **a** SPH modelling of water entry of an elastic wedge while the inherent features of free surface evolution, fluid-structure interaction, wave propagation and water jet are well captured (see: Liu and Zhang, Sci. China-Phys. Mech. Astron, 2019, 62:984701). **b** Simulated oil spill in water by using MPS method. Experimental results are compared. (see: Duan, Chen, Zhang and Wang, Comput. Meth. Appl. Mech. Engg, 2017, 320:133–161)

$$\frac{\partial f}{\partial t} + \boldsymbol{e} \cdot \frac{\partial f}{\partial \boldsymbol{x}} + \boldsymbol{a} \cdot \frac{\partial f}{\partial \boldsymbol{e}} = -\frac{1}{\tau}(f - f^{\mathrm{eq}}), \tag{4.4}$$

where $f(\boldsymbol{x}, \boldsymbol{e}, t)$ denotes the particle population (or velocity distribution function) with microscopic velocity $\boldsymbol{e}$ at position $\boldsymbol{x}$ and time $\boldsymbol{t}$ (see Fig. 4.2a, b), and $\boldsymbol{a}$ is the acceleration due to forces exerted on the particles. The first two terms on the left-hand side show a propagation process. On the right-hand side, we use BGK assumption, named after Bhatnagar, Gross and Krook. The BGK assumption implies f approaches the Maxwell-Boltzmann distribution, f^{eq}, after a large number of collisions preserving mass, momentum and kinetic energy conservation [8, 9]. τ is a relaxation time, which reflects the strength and frequency of the collisions and determines the viscosity of the fluid (to be shown in the rear part of this subsection). Therefore, this method is essentially a partial differential equation-based method, although it has strong particle kinetics background.

For computer-aided calculations, a discretization process is implemented as in Fig. 4.2c. The lattice shown has three major contents: the geometry of the control volume, the discrete microscopic velocity set (see $\boldsymbol{e}_i$ in the panel) and time step (δt). In standard LBM, it is supposed that the particle will jump to the neighbouring point at $\boldsymbol{x} + \boldsymbol{e}_i \delta t$ in each time step. For convenience, $\delta t = 1$ and the size of the lattice are chosen as the units of time and length, respectively. Equation (4.4) is then discretized (ignoring the volumetric force term) as

$$f_i(\boldsymbol{x} + \boldsymbol{e}_i \delta t, t + \delta t) - f_i(\boldsymbol{x}, t) = -\frac{1}{\tau}\left(f_i(\boldsymbol{x}, t) - f_i^{\mathrm{eq}}\right), \tag{4.5}$$

and the corresponding Maxwell distribution is

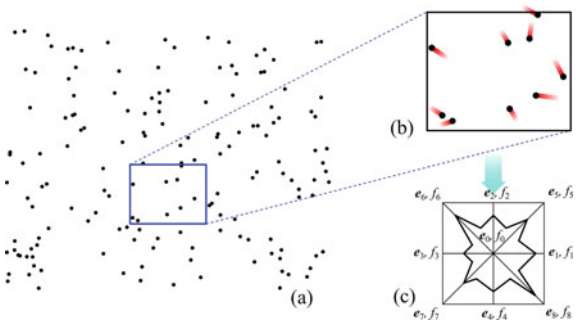

Fig. 4.2 Discretization of a particle system. **a** A particle system. The particles walk randomly, freely without interactions except when they collide with each other. **b** A volume element in the particle system. The space is discretized accordingly. **c** The microscopic velocity in panel (b) is discretized into nine velocities ($\boldsymbol{e}_i$, $i = 0, 1, 2 \ldots 8$) according to the lattice model chosen. Since two-dimensional space and nine discretized microscopic velocities are chosen, it is named as D2Q9 lattice. f_i denotes the particle population with microscopic velocity $\boldsymbol{e}_i$

$$f_i^{\mathrm{eq}}(\rho, \boldsymbol{u}) = \omega_i \rho(\boldsymbol{x}) \left[1 + 3\frac{\boldsymbol{e}_i \cdot \boldsymbol{u}}{c^2} + \frac{9(\boldsymbol{e}_i \cdot \boldsymbol{u})^2}{c^4} - \frac{3\boldsymbol{u}^2}{2c^2} \right]. \tag{4.6a}$$

The local macroscopic quantities can be easily assembled from the moments of f_i: density $\rho = \sum_i f_i$ and momentum $\rho \boldsymbol{u} = \sum_i f_i \boldsymbol{e}_i$. $c = 1/\sqrt{3}$ is the speed of sound on D2Q9 lattice, and

$$\omega_i = \begin{cases} 4/9, i = 0 \\ 1/9, i = 1, 2, 3, 4 \\ 1/36, i = 5, 6, 7, 8. \end{cases} \tag{4.6b}$$

Equation (4.5) is a typical LB equation. On numerical side, the calculations can be implemented quite easily, and that is one of the important reasons that LBM is applied in many fields explosively [10, 11].

The Chapman-Enskog expansion can be applied to recover N–S equations from Eqs. (4.5) and (4.6). To do so, we first introduce a multi-scale expansion:

$$f_i = f_i^{(0)} + \epsilon f_i^{(1)} + \epsilon^2 f_i^{(2)} + \cdots, \tag{4.7}$$

$$\partial_t = \partial_{t0} + \epsilon^2 \partial_{t1}, \partial_\alpha = \epsilon \partial_{\alpha 0}. \tag{4.8}$$

The subscripts t and α denote the derivatives with respect to time and position, respectively, and ϵ is a small number proportional to Knudsen number (the ratio between the mean free path of the particles and the characteristic length of the problem). Conduct Taylor expansion on Eq. (4.5) and use (4.8).

$$\begin{aligned} & f_i(x + e_i \delta t, t + \delta t) - f_i(x, t) \\ &= \left[\partial_t f_i + e_{i\alpha} \partial_\alpha f_i + \frac{1}{2} \left(\partial_t^2 f_i + 2 e_{i\alpha} \partial_t \partial_\alpha f_i + e_{i\alpha} e_{i\beta} \partial_\beta \partial_\alpha f_i \right) \right] \delta t \\ &= \Bigg[\epsilon \underbrace{\left(\partial_{t0} + e_{i\alpha} \partial_{\alpha 0} \right)}_{D_i^{(0)}} f_i + \epsilon^2 \partial_{t1} f_i + \\ & \frac{1}{2} \epsilon^2 \delta t \left(\partial_{t0}^2 + 2 e_{i\alpha} \partial_{t0} \partial_{\alpha 0} + e_{i\alpha} e_{i\beta} \partial_{\beta 0} \partial_{\alpha 0} \right) f_i + \cdots \Bigg] \delta t \\ &= \left[\epsilon D_i^{(0)} f_i + \epsilon^2 \partial_{t1} f_i + \epsilon^2 \frac{\delta t}{2} D_i^{(0)2} f_i + \cdots \right] \delta t. \end{aligned} \tag{4.9}$$

In the equation, Einstein's notation is used. Substituting (4.9), (4.7) to (4.5), we can get the following cascaded equations with the consideration of the coefficients of each order of ϵ:

$$\epsilon^0 : 0 = f_i^{(0)} - f_i^{\mathrm{eq}}, \tag{4.10}$$

$$\epsilon^1 : D_i^{(0)} f_i^{(0)} = -\frac{1}{\tau \delta t} f_i^{(1)}, \tag{4.11}$$

$$\epsilon^2 : \partial_{t1} f_i^{(0)} + D_i^{(0)} f_i^{(1)} + \frac{\delta t}{2}\left[D_i^{(0)}\right]^2 f_i^{(0)} = -\frac{1}{\tau \delta t} f_i^{(2)}. \tag{4.12}$$

On the other hand, it is easy to known

$$\begin{aligned} \sum_i f_i^{(0)} &= \sum_i f_i^{\mathrm{eq}} = \rho \\ \sum_i f_i^{(0)} \boldsymbol{e}_i &= \sum_i f_i^{\mathrm{eq}} \boldsymbol{e}_i = \rho \boldsymbol{u}, \end{aligned} \tag{4.13a}$$

and

$$\sum_i f_i^{(k)} = 0, \sum_i f_i^{(k)} \boldsymbol{e}_i = 0, \quad k > 0. \tag{4.13b}$$

Multiplying Eq. (4.11) by 1 and $\boldsymbol{e}_i$, respectively, and taking summation over $\boldsymbol{i}$, we can obtain the mass and momentum equation at the order of ϵ^1:

$$\partial_{t0} \rho + \partial_{\alpha 0} (\rho u_\alpha) = 0, \tag{4.14}$$

$$\partial_{t0} (\rho u_\alpha) + \partial_{\alpha 0}\, \pi_{\alpha\beta}^{(0)} = 0, \tag{4.15}$$

where $\pi_{\alpha\beta}^{(0)} = \sum_i e_{i\alpha} e_{i\beta} f_i^{(0)} = \rho u_\alpha u_\beta + p\delta_{\alpha\beta}$ is the zeroth-order momentum flux tensor, and $\delta_{\alpha\beta}$ is *Kronecker delta*, $p = c^2\rho$, respectively (please refer to Refs. [9, 10] for details). Equations (4.14) and (4.15) are Euler equations.

On ϵ^2 level, it can be easily derived following the above process:

$$\partial_{t1} \rho = 0, \tag{4.16}$$

$$\partial_{t1} (\rho u_\alpha) + \left(1 - \frac{1}{2\tau}\right) \partial_{\alpha 0}\, \pi_{\alpha\beta}^{(1)} = 0, \tag{4.17}$$

where $\pi_{\alpha\beta}^{(1)} = \sum_i e_{i\alpha} e_{i\beta} f_i^{(1)}$. To obtain the macroscopic meaning of $\pi_{\alpha\beta}^{(1)}$, (4.11) is treated

$$\begin{aligned} -\frac{1}{\tau\delta} \sum_i e_{i\alpha} e_{i\beta} f_i^{(1)} &= \partial_{t0} \sum_i e_{i\alpha} e_{i\beta} f_i^{(0)} + \partial_{\gamma 0} \sum_i e_{i\alpha} e_{i\beta} e_{i\gamma} f_i^{(0)} \\ &= \partial_{t0}\left(\rho u_\alpha u_\beta + c^2 \rho \delta_{\alpha\beta}\right) + \partial_{\gamma 0}\left[c^2 \rho \left(u_\alpha \delta_{\beta\gamma} + u_\beta \delta_{\gamma\alpha} + u_\gamma \delta_{\alpha\beta}\right)\right] \\ &= c^2\left[\partial_{t0}\rho + \partial_{\gamma 0}\left(\rho u_\gamma\right)\right]\delta_{\alpha\beta} + u_\beta[\partial_{t0}(\rho u_\alpha) + \partial_{\alpha 0} p] \\ &\quad + u_\alpha\left[\partial_{t0}\left(\rho u_\beta\right) + \partial_{\beta 0} p\right] + c^2 \rho\left[\partial_{\alpha 0} u_\beta + \partial_{\beta 0} u_\alpha\right] \end{aligned}$$

$$= c^2\rho\left[\partial_{\alpha 0}u_\beta + \partial_{\beta 0}u_\alpha\right] - \partial_{\gamma 0}\left(\rho u_\alpha u_\beta u_\gamma\right)$$
$$= c^2\rho\left[\partial_{\alpha 0}u_\beta + \partial_{\beta 0}u_\alpha\right] + O\left(M^3\right), \tag{4.18}$$

where M is Mach number. Further using the results in (4.14) and (4.15), (4.18) leads to

$$\pi_{\alpha\beta}^{(1)} = -\tau p\delta t\left(\partial_{\alpha 0}u_\beta + \partial_{\beta 0}u_\alpha\right), \tag{4.19}$$

after neglecting the $O\left(M^3\right)$ term.

Finally, we combine the equations on ϵ^1 and ϵ^2 scales and get the hydrodynamic equations

$$\frac{\partial\rho}{\partial t} + \nabla\cdot(\rho\boldsymbol{u}) = 0, \tag{4.20}$$

$$\frac{\partial(\rho u_\alpha)}{\partial t} + \nabla(\rho\boldsymbol{u}\boldsymbol{u}) = -\nabla p + \nabla\cdot\left[\rho\nu\left(\nabla\boldsymbol{u} + \nabla\boldsymbol{u}^T\right)\right]. \tag{4.21}$$

They also show the kinematic viscosity

$$\nu = c^2\left(\tau - \frac{1}{2}\right)\delta t. \tag{4.22}$$

As a matter of fact, in both (4.6) and (4.19), we use low Mach number assumption, which is fortunately the usual situation for acoustic phenomenon. On the other hand, with low Mach number condition, LBM is considered as a semi-incompressible flow solver.

4.2.2 *Implement of LBM Simulation*

In Eq. (4.5), only one relaxation time (τ) is presented for all f_i's relaxation and the approach is named as single relaxation time (SRT) LBM. The calculation generally goes in two steps:

$$f_i^+(\boldsymbol{x}, t) = f_i(\boldsymbol{x}, t) - \frac{1}{\tau}\left(f_i(\boldsymbol{x}, t) - f_i^{\mathrm{eq}}(\rho, \boldsymbol{u})\right), \tag{4.23a}$$

$$f_i(\boldsymbol{x} + \boldsymbol{e_i}\Delta t, t + \delta t) = f_i^+(\boldsymbol{x}, t), \tag{4.23b}$$

where the first one is collision step and the second one streaming step. The code is then organized as follows:

STEP 1: Initiate f_i on each grid node.
STEP 2: Calculate $\rho, \boldsymbol{u}$ (the moments of f_i) according to f_i.
STEP 3: Calculate equilibrium states, $f_i^{\mathrm{eq}}(\rho, \boldsymbol{u})$, according to (4.6a).
STEP 4: Implement collision step according to (4.23a).
STEP 5: Swap f_i between neighbouring grids following (4.23b).
STEP 6: Return STEP 2, if the stop criterion is not reached. Otherwise terminate the calculation.

The superior features of LBM will be introduced in the next section. Besides that, a well-proposed boundary condition should be applied in capturing acoustic phenomenon in numerical simulations. That is because the computational domain is usually truncated. In many acoustic simulations, the disturbance/sound propagated from the domain inside should penetrate the boundary without reflection, because the reflections could be of the same order as the real sound waves and contaminate the results [12]. The well-developed non-reflecting boundary conditions (NRBC) in traditional CFD can be applied in LBM. Although they must not be applicable, some of them do show great successes. Following the traditional classification, there are three categories of NRBC: open boundary (extrapolation method, EMBC), characteristics-based boundary condition (NSCBC) and absorbing layer boundary condition (ABC).

EMBC possibly was first proposed to remove the apparent influences of boundaries on flow field when the computational domain is truncated. In these domains, the influences of the model on the flow are hardly dissipated at the far end of the domain. For instance, the shedding vortex can reach the outlet boundary periodically in flow around a cylinder (see Fig. 4.3). Therefore, the quantities on the boundary are actually unknown for the calculations, leading to inapplicability of fixed velocity/pressure boundary condition. On inlet side, a poor-posed condition could lead to wrong results.

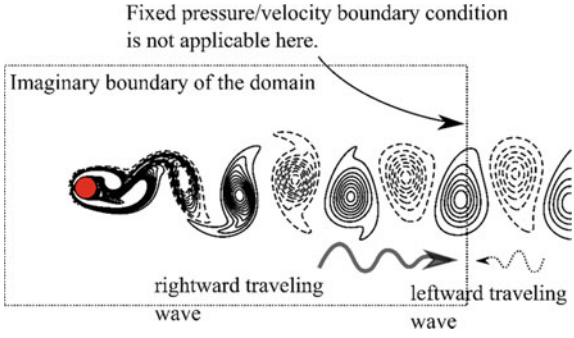

Fig. 4.3 An imaginary computational domain, where fixed pressure/velocity boundary condition cannot be applied on the outlet. The wavy arrows indicate the direction of flow information propagating. They could be from inside the domain (thick) or outside (thin) in real flow. The later one should be designed/modelled because it is unknown in calculations

Table 4.1 EMBC used by Chen [13]. The subscripts "$\boldsymbol{I}$", "$\boldsymbol{O}$" denote inlet and outlet of the domain, respectively

Boundary	Prescribed quantity on the boundary	Extrapolated quantity on the boundary
Inlet	$\boldsymbol{u}_I = \boldsymbol{U}$	$\rho_I = \rho_I^n = \frac{\bar{\rho}^n + \alpha_I \rho_I^{n-1}}{1+\alpha_I}$
Outlet	$p_O^n = \frac{p_O^{n-1} + \rho c(\bar{u}_n^n - \bar{u}_n^{n-1}) + \alpha_O \Delta t P}{1+\alpha_O \Delta t}$	$\boldsymbol{u}_O^n = \bar{\boldsymbol{u}}^n$

The overbars represent extrapolated variables, and the capitals are prescribed ones. The superscripts represent time step. α's are adjustable parameters. A damping effect is applied in p_O^n

A simple remedy is to extrapolate the variables, either macroscopic ones or mesoscopic ones (f_i's), near the boundary from in the domain. Table 4.1 shows an example applied by Chen [13], where the author extrapolates macroscopic variables. The mesoscopic quantities are then constructed according to non-equilibrium extrapolating method proposed by Guo et al. [14]. The unknown mesoscopic values are also constructed directly by using the extrapolation technique. Yu et al. [15] noticed the reflected wave can largely contaminate the meaningful pressure signal, and both equilibrium and deviated components of the distribution function are extrapolated. Smooth density distributions are obtained in the flows around cylinder and airfoil with different Reynolds numbers, respectively.

Another important NRBC roots in the disturbance/information propagation fundamentals in fluid. It is known that two symmetric or asymmetric waves meeting with each other on the boundary results in a Dirichlet boundary (either for pressure or velocity) [16]. It shares the common concept of characteristic line in fluid mechanics, so it is called NSCBC. The mathematical basis can be illustrated through one-dimensional derivation, also named as local one-dimensional inviscid (LODI) equation. The basic idea of NSCBC is presented as follows.

Supposing we have an unknown vector: $\boldsymbol{U} = [\rho, u_x]^{\mathrm{T}}$, the one-dimensional flow governing equations read

$$\frac{\partial}{\partial t}\boldsymbol{U} + \boldsymbol{\Gamma}_{\boldsymbol{x}} \frac{\partial}{\partial x}\boldsymbol{U} = 0$$

$$\boldsymbol{\Gamma}_{\boldsymbol{x}} = \begin{bmatrix} u_x & \rho \\ c^2/\rho & u_x \end{bmatrix} = \boldsymbol{S}^{-1}\boldsymbol{\Lambda}\boldsymbol{S}, \tag{4.24a}$$

$$\boldsymbol{\Lambda} = \begin{bmatrix} c+u_x & 0 \\ 0 & c-u_x \end{bmatrix}, \quad \boldsymbol{S} = \begin{bmatrix} \frac{c}{2\rho} & \frac{1}{2} \\ -\frac{c}{2\rho} & \frac{1}{2} \end{bmatrix}, \tag{4.24b}$$

Equation (4.24a) is recast as

$$\frac{\partial \rho}{\partial t} + \frac{\rho}{c}(L_1 + L_2) = 0, \tag{4.25a}$$

$$\frac{\partial u_x}{\partial t} + L_1 - L_2 = 0, \tag{4.25b}$$

$$L_1 = \frac{(u_x + c)}{2}\left(\frac{c}{\rho}\frac{\partial \rho}{\partial x} + \frac{\partial u_x}{\partial x}\right), \tag{4.25c}$$

$$L_2 = \frac{(u_x - c)}{2}\left(\frac{c}{\rho}\frac{\partial \rho}{\partial x} - \frac{\partial u_x}{\partial x}\right), \tag{4.25d}$$

where L_1 represents rightward travelling wave and L_2 leftward wave. We hope the flow state on the boundaries is influenced more from one side. For instance, in Fig. 4.3, the outlet is dominated by the flow upwind and an unknown incoming wave. Therefore, the leftward travelling wave should be suppressed artificially or modelled.

An example was presented by Izquierdo [17]. To obtain LODI equations, the authors used four inviscid flow equations (one mass, two momentum and one energy equations) and got four L_i's (refer to Eq. 4.25). For an outlet with a prescribed pressure (p_O), the incoming wave is modelled according to a relaxation process:

$$L_1(\boldsymbol{x}_b, t-1) = d[p(\boldsymbol{x}_b, t-1) - p_O], \tag{4.26a}$$

rather than the original one:

$$L_1^{\star}(\boldsymbol{x}_b, t-1) = (u_x - c)\left(\frac{\partial p}{\partial x} - \rho c \frac{\partial u_x}{\partial x}\right). \tag{4.26b}$$

In the equation, the subscripts b, O denote the variables on the boundary and the prescribed quantity, respectively, and d is a parameter. As $d = 0$ no information comes into the domain and the pressure is entirely floating. Nonzero d implies a partial reflective boundary condition and makes p varies around p_O. Subsequently, the macroscopic variables are calculated numerically:

$$\rho_b^t = \rho_b^{t-1} + L_1^{t-1} - \frac{1}{c^2}L_3^{t-1}, \tag{4.27a}$$

$$u_{bx}^t = u_{bx}^{t-1} - \frac{1}{2\rho c}\left[L_4^{t-1} - L_1^{t-1}\right], \tag{4.27b}$$

$$u_{by}^t = u_{by}^{t-1} - L_2^{t-1}. \tag{4.27c}$$

By using the quantities, the equilibrium function on the boundary is obtained as $f_i^{\mathrm{eq}+}(\rho_b, \boldsymbol{u}_b, t)$, which is further used to estimate the incoming distributions (through a virtual streaming step):

$$\begin{aligned} &f_i(\boldsymbol{x}_{b-1}, t+1) \\ &= -f_i(\boldsymbol{x}_{b-1}, t) + 2f_i^{eq+}(\boldsymbol{x}_b, t) + (2 - s_v)\Big[f_i(\boldsymbol{x}_{b-1}, t) - f_i^{eq+}(\boldsymbol{x}_b, t)\Big], \end{aligned} \tag{4.28}$$

where the first term is antibounce back, the second term is for the Dirichlet pressure setting, and the last one is a correction to eliminate second-order error term (s_v is a dissipation parameter). $\boldsymbol{e}_{\bar{i}} = -\boldsymbol{e}_i$.

A third group of NRBC is ABC (or sponge layer condition), the key idea of which is to introduce extra damping effect in a zone around the boundary. Any waves will be dissipated gradually in this zone without reflection. Its ancestor can be also found in traditional CFD model [12] and the governing equation generally reads

$$\frac{\partial \boldsymbol{U}}{\partial t} + N(\boldsymbol{U}) = -\sigma(x)(\boldsymbol{U} - \boldsymbol{U}_O), \tag{4.29}$$

where N represent a non-linear operator and $\sigma(x)$ a spatially varying friction coefficient. Provided $\sigma(x)$ is large enough, the source term will drive $\boldsymbol{U}$ to $\boldsymbol{U}_O$ quickly. Therefore, to the absorbing zone, both incoming and reflected waves will be dissipated, no matter what kind of numerical boundary is imposed.

Xu and Sagaut gave a detailed analysis on the implement of ABC in LBM [18]. The LB equation in ABC zone is presented as

$$\begin{aligned} &f_i(\boldsymbol{x} + \boldsymbol{e}_i\delta t, t + \delta t) - f_i(\boldsymbol{x}, t) \\ &= -\frac{1}{\tau}\left(f_i(\boldsymbol{x}, t) - f_i^{\mathrm{eq}}\left(\rho^*, \boldsymbol{u}^*\right)\right) + \chi\left(f_i^{\mathrm{ref}}(\boldsymbol{x}, t) - f_i^*(\boldsymbol{x}, t)\right), \end{aligned} \tag{4.30}$$

where χ characterizes the absorbing strength in the zone. $f_i^{\mathrm{ref}}(\boldsymbol{x}, t)$ denotes the reference state of $f_i(\boldsymbol{x}, t)$, and $f_i^*(\boldsymbol{x}, t)$ the possible representations of distribution functions. Xu and Sagaut [18] analysed and compared several choices of $f_i^{\mathrm{ref}}(\boldsymbol{x}, t)$ and $f_i^*(\boldsymbol{x}, t)$. They suggest:

$$f_i^{\mathrm{ref}}(\boldsymbol{x}, t) = f_i^{\mathrm{eq}}(\rho_O, u_O, t), \tag{4.31a}$$

$$f_i^*(\boldsymbol{x}, t) = f_i^{\mathrm{eq}}(\rho, \boldsymbol{u}, t). \tag{4.31b}$$

In the equations, modified macroscopic density and velocity (ρ^* and $\boldsymbol{u}^*$) are applied considering the source term in Eq. (4.30) (the last one). They followed Guo et al. [19] to get the macroscopic quantities:

$$\rho^* = \sum_i f_i + \frac{1}{2}\sum_i \chi\left(f_i^{\mathrm{eq}}(\rho_O, u_O, t) - f_i^{\mathrm{eq}}(\rho, \boldsymbol{u}, t)\right), \tag{4.32a}$$

$$\rho^* \boldsymbol{u}_\alpha^* = \sum_i \boldsymbol{e}_{i\alpha} f_i + \frac{1}{2}\sum_i \chi \boldsymbol{e}_{i\alpha}\left(f_i^{\mathrm{eq}}(\rho_O, u_O, t) - f_i^{\mathrm{eq}}(\rho, \boldsymbol{u}, t)\right). \tag{4.32b}$$

The equations recover (4.29) and have a known mapping relation $\sigma_{\mathrm{LBM}} \equiv g(\tau, \chi)$. It is found the sound speed is also tuned due to the source term; however, we do not really care about the physics in the absorbing layer and the flow in it can be ignored.

At last, given $\sigma_{\mathrm{LBM}}(x)$, such as $\sigma_{\mathrm{LBM}}(x) = \frac{3125(L-x)(x-x_0)^4}{256(L-x_0)}$ (where L is the width of the absorbing layer and x_0 is the inner most position of the layer), local damping parameter can be achieved: $\chi(x) = g^{-1}(\sigma_{\mathrm{LBM}}(x), \tau)$.

The above methods are chosen in various studies according to the specific purposes, respectively. On the other hand, some of them can be combined with each other. In Fig. 4.4, a comparison of the boundary condition is presented, where panel (a) shows the density distribution slightly before the wave reaches the boundary layer. The (fully reflective) wall boundary (Fig. 4.4b) and Xu's (Fig. 4.4d) boundary [18] are the worst and best, respectively, for absorbing. A virtual layer of fluid with tuned viscosity is imposed around the computational domain in Fig. 4.4c. The viscosity profile in the boundary zone is of cosine: $\nu_{ABC} = \left[\frac{\nu-\nu_O}{2}\left(1+\cos\frac{\pi x}{L}\right)+\nu_O\right]$, where $\nu_O > \nu$ is an increased virtual viscosity in absorbing layer. The sound wave is reflected partially on this boundary.

In this section, some basic ingredient of LBM is introduced, which might help the readers for their first LBM codes. LBM is actually considered as a general CFD solver in wide range of academic and applied fields, where free surface, turbulent and

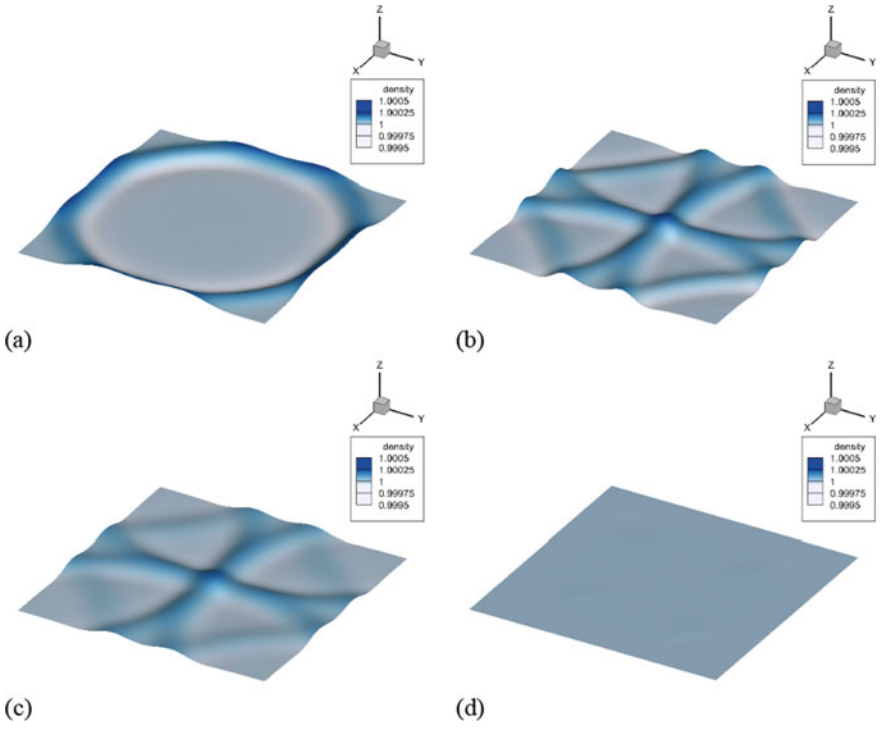

Fig. 4.4 Absorption of Gaussian density wave on the computational domain boundary. **a** Density distribution slightly before the density/pressure wave reaches the boundary (the "initial state"). Density distribution after the wave is "reflected" by **b** solid wall, **c** absorbing layer with tuned viscosity, **d** Xu & Sagaut's ABC

thermal effects might be concerned. There are also fast improvement and extension on the subjects in the very recent years. The readers are strongly suggested referring to relative publications for details, some of which are presented in the context.

4.3 Acoustic Studies by Using LBM

In the presenting section, we mentioned the flow fundamentals for aeolian tones, which theoretically can be explored by using proper flow model. With consideration of environment protection, aero/hydro-acoustics emerges as one of the most important subjects in modern aircraft, automobile and high-speed train industry. Noise control of marine vehicles is also required urgently for animal health. On the other hand, acoustic techniques are also widely used in the frontier of precise machinery, such as acoustic levitation, acoustic tweezer and cavitation bubble manipulation.

Computational aeroacoustics (CAA) has been developed as an efficient tool for the studies [5]. Deviating from normal CFD, there are special requirements for CAA. For instance, the unsteadiness and scale separation require high temporal and special resolution of the numerical model; the magnitude of acoustic wave is far smaller than the flow itself, which places stringent requirement on numerical accuracy. Therefore, two types of approaches are developed: direct numerical simulation (DNS) and indirect (hybrid) one. Sound and flow are computed together in the former one; only flow scale is resolved in numerical in the later one, while the propagation of sound is computed by using simplified model (like linearized Euler equation). In this section, the numerical feature of LBM is introduced, followed by the applications on both direct and indirect simulation levels.

4.3.1 The Dispersion Relation in LBGK Model

Interestingly, LBM is quite suitable for the sound capture in low speed (semi-incompressible) flow. In fact, one who conducts LBM simulation can always observe acoustic/pressure waves shortly after the calculation is started. The relative studies in fact have been carried out in the last decade, where the stability of the method is focused in. The propagation and development of disturbance are considered in both quiescent and flowing fluid. The validation of LBM on acoustic simulation is directly demonstrated in the framework of mathematics, or specifically, by using von Neumann analysis.

As described by Sagaut and Cambon [20], the N–S equations imply that the fluctuation can be divided into acoustic (longitudinal) and vorticity (shear) mode, which correspond to compressible and incompressible motion, respectively. There is another energy (entropic) mode, and it is neglected in LBM analysis because we normal focus on isothermal processes and the variation of entropy is neglected. Simplified N–S equations lead to a dissipation parameter and dispersion relation:

$$\alpha = \frac{k^2\nu'}{2}, \quad \frac{\omega}{k} = c\sqrt{1 + \frac{k^2\nu'^2}{4c^2}}. \tag{4.33}$$

The details can be found in the relative textbooks and references [2, 16, 21]. The results will be compared simply with the LBM results obtained in the rear part of this section.

The key idea of the von Neumann analysis is described as: tracking the evolution of fluctuations with various frequency in a numerical approach. Fortunately, in many circumstances, the speed of sound is much higher than mean flow (low Mach number assumption: $M \ll 1$) and the sound propagation and flow are decoupled with each other [see also Eq. (4.3)]. Then we focus on sound capture in media at rest. Meanwhile, with infinitesimally weak fluctuation, the governing equation can be linearized, which makes feasibility for the analysis. Both the macroscopic and mesoscopic quantities can be decomposed as a mean and fluctuating part, respectively:

$$\rho(\boldsymbol{x}, t) = \rho_0 + \rho'(\boldsymbol{x}, t), \tag{4.34a}$$

$$p(\boldsymbol{x}, t) = p_0 + p'(\boldsymbol{x}, t), \tag{4.34b}$$

$$\boldsymbol{u}(\boldsymbol{x}, t) = \boldsymbol{0} + \boldsymbol{u'}(\boldsymbol{x}, t), \tag{4.34c}$$

$$f_i(\boldsymbol{x}, t) = F_i^{\mathrm{eq}} + f_i'(\boldsymbol{x}, t), \tag{4.34d}$$

$$\rho_0 \gg \rho'(\boldsymbol{x}, t), \quad p_0 \gg p'(\boldsymbol{x}, t), \quad \boldsymbol{u'} \ll 1,$$

noting ideal gas equation of state is applicable in isothermal LBM (see Sect. 4.1): $p = c^2\rho$ and $p = \rho/3$ in D2Q9 lattice model. F_i^{std} denotes the distribution function for resting state. According to Eq. (5.6),

$$F_i^{\mathrm{std}} = F_i^{\mathrm{eq}}(\rho_0, \boldsymbol{0}) = \omega_i \rho_0, \tag{4.35}$$

where the non-linear parts are dropped off. It is worthy knowing that f_i' corresponds to unsteady flow. Without losing generality, $f_i' = f_i^{\circ} \mathrm{e}^{i(\omega^\star t - \boldsymbol{k}\cdot\boldsymbol{x})}$, where $\omega^\star$ is angular speed and $\boldsymbol{k} = 2\pi/\lambda\hat{\boldsymbol{k}}$ the wavenumber vector, λ is the wave-length. Calculate the moments:

$$\begin{aligned}\begin{bmatrix} \rho \\ \rho u' \end{bmatrix} &= \begin{bmatrix} \rho_0 \\ 0 \end{bmatrix} + \begin{bmatrix} \rho^{\circ} \\ \rho_0 \boldsymbol{u}^{\circ} \end{bmatrix} \mathrm{e}^{(\omega^\star t - \boldsymbol{k}\cdot\boldsymbol{x})} \\ &= \begin{bmatrix} \sum\limits_i F_i^{\mathrm{std}} \\ \sum\limits_i F_i^{\mathrm{std}} \boldsymbol{e}_i \end{bmatrix} + \begin{bmatrix} \sum\limits_i f_i^{\circ} \\ \sum\limits_i f_i^{\circ} e \end{bmatrix} \mathrm{e}^{(\omega^\star t - \boldsymbol{k}\cdot\boldsymbol{x})},\end{aligned} \tag{4.36}$$

and the equilibrium state is expended as

$$f_i^{\mathrm{eq}}\left(F_j^{\mathrm{std}}+f_j'\right)=F_i^{\mathrm{eq}}(\rho_0,\mathbf{0})+\left.\frac{\partial f_i^{\mathrm{eq}}}{\partial f_j}\right|_{f_j=F_j^{\mathrm{std}}} f_j'+O\left(f_j^{\circ 2}\right)$$
$$=\omega_i\rho_0+\underbrace{\omega_i\left(\rho'+3\frac{\rho_0\boldsymbol{u}'\cdot\boldsymbol{e}_i}{c^2}\right)}_{f_i'^{\mathrm{eq}}}+\cdots. \tag{4.37}$$

Substitute Eq. (4.37) into (4.5), we obtain

$$f_i'(\boldsymbol{x}+\boldsymbol{e}_i,t+1)=\left(1-\frac{1}{\tau}\right)f_i'(\boldsymbol{x},t)+\frac{1}{\tau}f_i'^{\mathrm{eq}}(\boldsymbol{x},t), \tag{4.38a}$$

and by using sinusoidal wave denotation,

$$f_i^{\circ}\mathrm{e}^{i(\omega^\star-\boldsymbol{k}\cdot\boldsymbol{e}_i)}=\left(1-\frac{1}{\tau}\right)f_i^{\circ}+\frac{\omega_i}{\tau}\left(\sum_j f_j^{\circ}+\frac{3\boldsymbol{e}_i}{c^2}\cdot\sum_j \boldsymbol{e}_j f_j^{\circ}\right), \tag{4.38b}$$

Set $\boldsymbol{f}^{\circ}=\left[f_0^{\circ},f_1^{\circ},\ldots,f_8^{\circ}\right]^{\mathrm{T}}$, the equations can be re-organized as

$$\mathrm{e}^{i\omega^\star}\boldsymbol{f}^{\circ}=\boldsymbol{A}^{-1}\left(\boldsymbol{I}-\frac{1}{\tau}\boldsymbol{B}\right)\boldsymbol{f}^{\circ}=\boldsymbol{M}\boldsymbol{f}^{\circ},$$
$$\boldsymbol{A}=\mathrm{diag}\left[1,\mathrm{e}^{-i\boldsymbol{k}\cdot\boldsymbol{e}_1},\mathrm{e}^{-i\boldsymbol{k}\cdot\boldsymbol{e}_2},\ldots,\mathrm{e}^{-i\boldsymbol{k}\cdot\boldsymbol{e}_8}\right], \tag{4.38c}$$

which leads to an eigenvalue problem. The dispersion relation can be obtained through the characteristic equation:

$$\det\left(\boldsymbol{M}-\boldsymbol{I}\mathrm{e}^{i\omega^\star}\right)=g\left(\omega^\star,\boldsymbol{k},\tau\right)=0. \tag{4.39}$$

Generally speaking, an analytical solution cannot be obtained easily. In fact, the above introduction only gives a very simple route for the dispersion relation. A more complicated version is given by Marie [22] and Lallemand [23], respectively, who considered the non-linear terms in f_i^{eq}'s. Figure 4.5 shows the relations indicating ideal speed of sound and dissipation can be preserved in small wavenumber. It is suggested roughly 12 points should be applied to capture sound propagation properly.

4.3.2 Applications of LBM in CAA

In the recent decades, LBM has already been demonstrated as a great candidate for acoustic simulations. The studies range on three levels: fundamentals and techniques, modelled flow simulations and industrial applications.

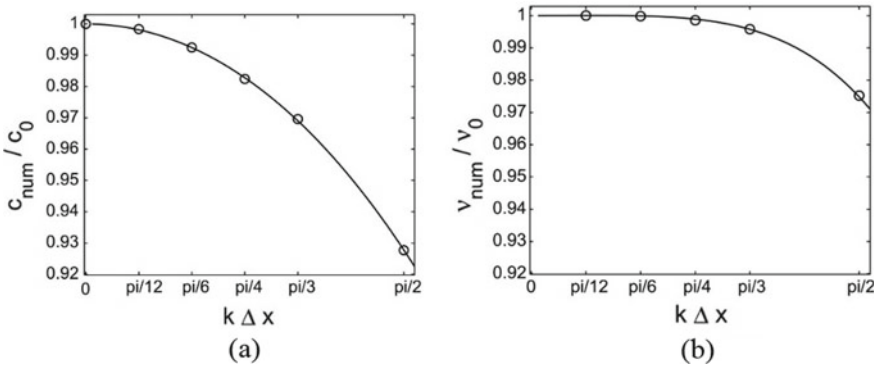

Fig. 4.5 The speed of sound (dispersion relation) (**a**) and dissipation (**b**) variations against wave number. The curves indicate the theoretical results and the symbols are numerical ones [22]

On technical levels, there are some valuable developments on the elementary issues about LBM simulation besides the aforementioned dispersion analyses and NRBC's. These work supplies more feasibility and accuracy for the simulations.

- Sound source in LBM. They could be modelled as solid boundary motion or point pressure oscillation. Many sounds are emitted from wall oscillation. Especially when the wall geometry should be concerned, it is naturally that we simply impose oscillating motion on a wall. Barrios and Rechtman [24] added additional source term, $Q_i = \omega_i P e_{iy}$, in the collision step [see Eq. (4.23a)] on the lattice coinciding with the acoustic source. The subscript y denotes the vibrating direction, and $P = P_0 \cos \omega t$. The modification leads to instantaneous input of momentum from the wall. Chen and Ren [25] directly imposed oscillating pressure on the boundary, and standing acoustic wave could be achieved. On the other hand, point sources are interested in many circumstances. They are valuable for both numerical models and many industrial designs. One can of course set some points in a simple manner like $f_i(\boldsymbol{x}, t) = f_i^{\mathrm{eq}}(\rho_0 \cos \omega t, \boldsymbol{0})$. However, the flow/wave information is entirely isolated from the points. Viggen [26] extended the idea of Barrios and Rechtman's [24] to multipole acoustic sources, by which the simulated noise is greatly decreased.
- In Sect. 5.2.1, we derive the dispersion relation of BGK-LBM. It is shown that BGK-LBM still suffers from some drawbacks, such as anisotropic and conditional stability [22, 23]. One of the successful improvements is multiple-relaxation time LBM (MRT-LBM), where the relaxation of moments/macroscopic quantities is applied rather than the density populations in collision step [23]. A relaxation time matrix is proposed,

$$\boldsymbol{T} = \boldsymbol{M}^{-1} \boldsymbol{\Lambda} \boldsymbol{M}, \boldsymbol{\Lambda} = \mathrm{diag}(s_0, s_1, \ldots, s_8), \tag{4.40a}$$

and the collision process is undergone on the corresponding moment space:

$$\boldsymbol{m} = \boldsymbol{M}\boldsymbol{f}, \quad \boldsymbol{f} = [f_0, f_1, \ldots, f_8]^{\mathrm{T}}. \tag{4.40b}$$

In MRT-LBM, the relaxation of the density distributions is coupled; however, the speed of it can be adjusted independently. In Eq. (4.40a), $s_0 = s_1 = \ldots = s_8 = 1/\tau$ recovers the SRT-LBM. By tuning the bulk damping property of the fluid (in numerical calculations), the stability of the calculation is strengthened. Filter techniques are further proposed [27, 28] to remedy the overdamping on acoustic waves in MRT-LBM.

In aeroacoustics, there are bunch of standard flows which result in sound emission. They basically relate to aeroacoustic theories and also have realistic meanings. For instance, the Lighthill equation describes a flow without solid boundary, which can occur in free jet flow. To simulate high Reynolds number (characterizing the ratio between kinetic energy and viscous dissipation of the flow) jet flow can not only be used to explore fluid mechanics but also assess numerical method. Coupled with certain turbulence model, such as VLES, RNG-$k-\varepsilon$ model, SRT-LBM can well predict the turbulent flow ejected from a nozzle [29, 30]. The results show the prior feature of LBM on capturing both flow details and sound signals.

Guo and Chen [31] conducted LBM simulation on two-dimensional vortex motion and investigated the sound emission. In their studies, a vortex pair (VP), either co-rotating or counter-rotating, is set in a space with or without wall boundary. Two approaches were applied to obtain the far field sound: direct measurement from numerical results and calculations according to Lighthill theory. Although large Reynolds number was applied, which traditionally is treated with simple inviscid flow model, the results showed a subtle viscous influence on the vortices motion, and therefore influence the sound emission. Recalling the mathematical analysis in Sect. 4.2.1, it is not surprising that directly simulated results agree with the theoretical results on both mean flow and disturbance propagation (see Figs. 4.5 and 4.6).

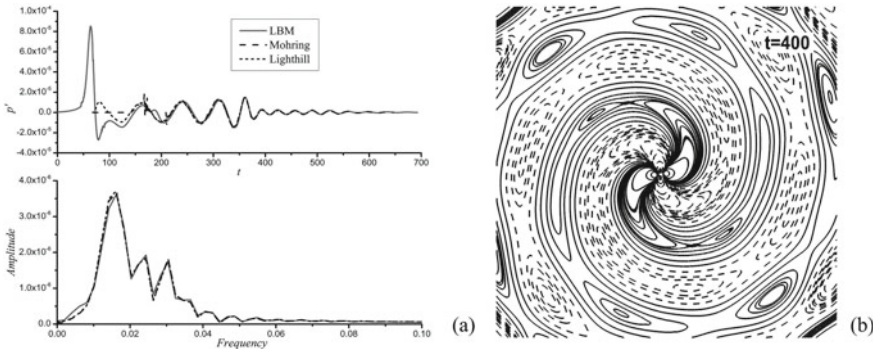

Fig. 4.6 LBM simulation of vortex pair dynamics in a free space and the sound emission. **a** Far field sound pressure oscillation obtained by direct measurement in numerical results and theoretical predictions (upper part). The spectra of the signals are compared in the lower part. **b** The sound pressure distribution of a co-rotating vortex pair in free space [31]

LBM simulation has been applied in industry. As proposed in the previous part, turbulent jet flow is well studied in CAA, which has important practical purposes, such as assessment of noise level in jet propelling of airplane. The similar numerical approaches are used in many other problems. Khorrami et al. [32] conducted large-scale numerical simulations on the flow and noise performance of Gulfstream aircraft model. Compared to experiments and third party numerical results, the LBM simulation is demonstrated very accurate and effective. In the simulations, flowing $M = 0.2$ and the flap deflected 39° are applied. The former condition almost touches the LBM's low Mach number limit, and the later one is obviously very tough for CFD technique due to severe flow separation. Besides that, the flows at the flap inboard and outboard tips and main landing gear are captured correctly, which is considered as main noise sources on landing phase of aircraft. The authors also applied Ffowcs-Williams and Hawkings acoustic analogy approach to the numerical results and obtained good agreement on far-field noise prediction.

Coupled with various turbulence model, LBM is validated as a powerful tools addressing industrial flows and noise predictions.

4.4 LB Simulation in Acoustic Levitation and Second-Order Acoustic Flow

Buick et al. showed LBM can well reproduce non-linear acoustic effects, which is not surprise concerning its dispersion and dissipation features [2]. For large-scale flows, to capture their acoustic footprint depends also on turbulence model as aforementioned: in fact that is a key issue for the accuracy. On the other hand, more precise control of sound phenomena, such as propagation, reflection and deflection, also has plenty of potentials for application. The flows in these circumstances are normally laminar and many theoretical models were actually proposed. On the numerical side, the requirement for dissipation and dispersion feature makes LBM very applicable.

Haydock and Yeomas [33, 34] firstly used LBM to reproduce acoustic streaming correctly. In their study, a simple version of BGK-LBM is applied for classical Rayleigh streaming and Eckart streaming. Both of the streaming originates from attenuation, and they can be illustrated through a simple model as follows.

Suppose the oscillation of the fluid element is damped along the wave line and has a general form of $u_x = U\mathrm{e}^{-\alpha x}\cos(\omega t - kx)$. It leads to Reynolds stress and a pressure gradient:

$$\partial_x P_2 = F_x = -\rho_0\langle 2u_x u_x\rangle = \rho_0\alpha U^2\mathrm{e}^{-2\alpha x}, \tag{4.41}$$

where the point bracket denotes time average value. It implies a steady flow. Obviously, the flow is of second order. If the dissipation is mainly in the boundary layer near a wall, the streaming driven by the Reynolds stress is call Rayleigh streaming; if the dissipation occurs in the bulk, Eckart streaming is resulted in. It is shown that both

time dependent first order flow and the streaming are predicted well by using LBM correctly. Furthermore, Haydock and Yeomas [34] and Rafat et al. [35] extended the method to more complicated geometries, which is not well described by theories.

Following their prediction of LBM targeting detailed acoustic simulation, Haydock [36] further investigated acoustic radiating forces on a (two-dimensional) cylinder. Full N–S equations were simulated through LBM in low viscosity regime. A viscous penetrating depth was introduced: $\beta^{-1} = \sqrt{2\nu/\omega}$. The results show that the deviation of acted force on the cylinder against inviscid prediction vanishes linearly as $(a\beta)^{-1}$ approaches zero, where a is radius of the cylinder. By setting the cylinder in a standing acoustic wave, its trajectory was presented, which approaches a pressure node. The model was further set in a channel, where Rayleigh streaming was induced by longitudinal standing wave. The viscous force is dominant and also leads to transversal motion of the cylinder to the centre of the channel. Barrios and Rechtman [24] simulated acoustic levitation in details by using LBM. The density ratio, levitator geometry and acoustic strength are investigated. It is interesting that two pressure nodes are found as a rounded cavity is used, which destabilizes the cylinder oscillation. Barrios and Rechtman also propose that, although larger oscillation and non-periodic motion of the "levitated" particle are obtained for rounded cavity, it is easily to be levitated in weak sound waves. Chen and Ren [25] compared the details of simulated acoustic flow and theoretical predictions around a cylinder. Their results show that the viscous flow in boundary layer is discerned clearly from the periodic far-field flow. The later can be described well by using potential flow theory. The measured boundary thickness fulfils the theoretical prediction very well. In the time averaged flow field, one or two layers of steady recirculation are found depending on $(a\beta)^{-1}$.

4.5 Summary

In this chapter, we introduce the fundamentals, implement issues and applications of lattice Boltzmann method in acoustics. It should be said that lattice Boltzmann method is comparatively easy for coding and of high efficiency for parallel computing. It could be considered as a substitutional approach for N–S equation-based computational methods and beyond. By using von Neumann analysis, we show that correct dispersion relation can be obtained when the wavenumber is small. Of course, recently improvement on lattice Boltzmann method allows further lower grid resolution for acoustic simulations. The prior features of the method lay solid basis for acoustic simulation, which includes both aeolian tones and precise sound wave reproducing. For the later one, non-linear motions may play important roles. On acoustic levitations, lattice Boltzmann simulations show the viscous forces become more salient as the viscous penetrating depth grows. As well, interesting results are revealed for cavity geometry, etc. Besides the theoretical study, lattice Boltzmann simulation makes more precise design for levitation equipment and deeper understanding of physics is presented available.

References

1. D.L. Landau, E.M. Lifshitz, *Fluid Mechanics* (Butterworth-Heineman, Oxford, 1999)
2. J.M. Buick, C.L. Buckley, C.A. Greated, J. Gilbert, Lattice Boltzmann BGK simulation of nonlinear sound waves: the development of a shock front. J. Phys. A: Math. Gen. **33**, 3917–3928 (2000)
3. M. Goldstein, *Aeroacoustics* (McGraw-Hill Inc., New York, 1976)
4. J.E. Ffowcs-Williams, Aeroacoustics. Annu. Rev. Fluid Mech. **9**, 447–468 (1977)
5. M. Wang, J.B. Freund, S.L. Lele, Computational prediction of flow-generated sound. Annu. Rev. Fluid Mech. **38**, 483–512 (2006)
6. S.S. Sadhal, Acoustofluidics 15: streaming with sound waves interacting with solid particles. Lab Chip **12**, 2600–2611 (2012)
7. M. Settnes, H. Bruus, Forces acting on a small particle in an acoustical field in a viscous fluid. Phys. Rev. E **85**, 016327 (2012)
8. C.K. Aidun, J.R. Clausen, Lattice-Boltzmann method for complex flows. Annu. Rev. Fluid Mech. **42**, 437–472 (2010)
9. S. Chen, G.D. Doolen, Lattice Boltzmann method for fluid flows. Annu. Rev. Fluid Mech. **30**, 329–364 (1998)
10. Z. Guo, C. Shu, *Lattice Boltzmann method and its applications in engineering* (World Scientific Publishing, Singapore, 2013)
11. H. Huang, M.C. Sukop, X.-Y. Lu, *Multiphase lattice Boltzmann methods* (Wiley, Singapore, 2015)
12. T. Colonius, Modeling artificial boundary conditions for compressible flow. Annu. Rev. Fluid Mech. **36**, 315–345 (2004)
13. X.-P. Chen, Applications of lattice Boltzmann method to turbulent flow around two-dimensional airfoil. Engg. Appl. Compt. Fluid Mech. **6**, 572–580 (2012)
14. Z. Guo, C. Zheng, B. Shi, Non-equilibrium extrapolation method for velocity and pressure boundary conditions in the lattice Boltzmann method. Chin. Phys. **11**, 366–374 (2002)
15. D. Yu, R. Mei, W. Shyy, Improved treatment of the open boundary in the method of lattice Boltzmann equation. Prog. Comput. Fluid Des. **5**, 3–12 (2003)
16. E.M. Viggen, Sound waves, in *The Lattice Boltzmann* (Springer Nature, Switzerland, 2017), pp. 493–529
17. S. Izquierdo, N. Fueyo, Characteristic nonreflecting boundary conditions for open boundaries. Phys. Rev. E **78**, 046707 (2008)
18. H. Xu, P. Sagaut, Analysis of the absorbing layers for the weakly-compressible lattice Boltzmann method. J. Comput. Phys. **245**, 14–42 (2013)
19. Z. Guo, C. Zheng, B. Shi, Discrete lattice effects on the forcing term in the lattice Boltzmann method. Phys. Rev. E **65**, 046308 (2002)
20. P. Sagaut, C. Cambon, *Homogeneous Turbulence Dynamics* (Cambridge University Press, Cambridge, 2008)
21. A. Wilde, Calculation of sound generation and radiation from instationary flows. Comput. Fluids **35**, 986–993 (2006)
22. S. Marie, D. Ricot, P. Sagaut, Comparison between lattice Boltzmann method and Navier–Stokes high order schemes for computational aeroacoustics. J. Comput. Phys. **228**, 1056–1070 (2009)
23. P. Lallemand, L.-S. Luo, Theory of the lattice Boltzmann method: dispersion, dissipation, isotropy, Galilean invariance, and stability. Phys. Rev. E **61**, 6546–6562 (2003)
24. G. Barrios, R. Rechtman, Dynamics of an acoustically levitated particle. J. Fluid Mech. **596**, 191–200 (2008)
25. X.-P. Chen, H. Ren, Acoustic flows in viscous fluid: a lattice Boltzmann study. Int. J. Numer. Methods Fluids **79**, 183–198 (2015)
26. E.M. Viggen, Acoustic multipole sources for the lattice Boltzmann method. Phys. Rev. E **87**, 023306 (2013)

27. D. Ricot, S. Marie, P. Sagaut, C. Bailly, Lattice Boltzmann method with selective viscosity filters. J. Comput. Phys. **228**, 4478–4490 (2009)
28. S. Marie, X. Gloerfelt, Adaptive filtering for the lattice Boltzmann method. J. Comput. Phys. **333**, 212–226 (2017)
29. F.D. da Silva, C. J. Deschamps, Assessment of jet-plate interaction noise using the lattice boltzmann method, in *21st AIAA/CEAS Aeroacoustics Conference* (AIAA 2015-2207), Dallas, TX (2015)
30. D. Casalino, S.K. Lele, *Lattice-Boltzmann simulation of coaxial jet noise generation* (Center for Turbulence Research, Stanford, 2014)
31. R.-Q. Guo, X.-P. Chen, Sound generation by two dimensional vortex pair motion and the influence of viscosity. Comput. Math Appl. **78**, 2761–2771 (2019)
32. M.R. Khorrami, E. Fares, D. Casalino, Towards full aircraft airframe noise prediction, in *20th AIAA/CEAS Aeroacoustic Conference* (AIAA 2014-2480), Atlanta, GA (2014)
33. D. Haydock, J.M. Yeomas, Lattice Boltzmann simulations of acoustic streaming. J. Phys. A: Math. Gen. **34**, 5201–5213 (2001)
34. D. Haydock, J.M. Yeomas, Lattice Boltzmann simulations of attenuation-driven acoustic streaming. J. Phys. A: Math. Gen. **36**, 5683–5694 (2003)
35. Y. Rafat, K. Habibi, L. Mongeau, Direct numerical simulations of acoustic streaming in standing wave tubes using the lattice Boltzmann method. Proc. Mtgs. Acoust. **19**, 045006 (2013)
36. D. Haydock, Lattice Boltzmann simulations of the time-averaged forces on a cylinder in a sound field. J. Phys. A: Math. Gen. **38**, 3265–3277 (2005)